CrystEngComm

Accepted Manuscript

ROYAL SOCIETY OF CHEMISTRY

www.rsc.org/crystengcomm

Journal Name

ARTICLE

Photoluminescence Enhancement Induced by a Halide Anion Encapsulation in a Series of Novel Lanthanide(III) Coordination Polymers

Received 00th January 20xx,
Accepted 00th January 20xx

DOI: 10.1039/x0xx00000x

www.rsc.org/

Cong Xu [a], Alexander M. Kirillov [b], Yubo Shu [a], Yan Liu [a], Lirong Guo [a], Lizi Yang [a], Wei Dou [a], Wei Liu [a], Chunyang Chen [a], Xin Huang [a], Jiayao Zhang [a], and Weisheng Liu [a]*

Nine new isostructural 2D lanthanide(III) coordination polymers (Ln-CPs) with a general formula of $\{[Ln(Bcpi)_2(H_2O)]Br_xCl_{1-x}\cdot(H_2O)\}_n$ {Ln = Eu (**1–3**), Tb (**4–6**) and Gd (**7–9**); x = 0, 0.5, 1; Bcpi = 1,3-bis(4-carboxyphenyl)imidazolium} were synthesized by hydrothermal reactions and fully characterized. Single-crystal X-ray structural analysis revealed that this series of Ln-CPs displays 1D channel motifs with encapsulated halide anions, whereas their overall 2D metal-organic networks can be topologicallly classified as the **kgd** underlying nets. Compounds **1–3** show five characteristic emission lines with maxima at 579, 591, 617, 652 and 701 nm owing to the $^5D_0 \rightarrow {}^7F_J$ (J = 0-4) transitions, respectively. Besides, compounds **4–6** exhibit four sharp peaks at 487, 544, 582 and 619 nm resulting from the $^5D_4 \rightarrow {}^7F_J$ (J = 6-3) transitions. The emission spectra indicate that the halide anions captured in the porous structure could induce the enhancement of photoluminescence. Furthermore, the emission strength and quantum yield increase when the encapsulated choride anions are replaced by bromide anions. In addition, by using the *in situ* doping method, a series of heterometallic Tb/Eu coordination polymers $\{[Tb_{1-x}Eu_x(Bcpi)_2(H_2O)]Cl\cdot(H_2O)\}_n$ (**10**) with a different content of metals {x = 0.001, 0.002, 0.005, 0.01, 0.02, 0.03, 0.04, 0.05, 0.1 and 0.2} were generated, which are tunable yellow light luminescent materials and simultaneously display two major emission bands at 612 and 545 nm due to Eu(III) and Tb(III) emission, respectively.

Introduction

The design and synthesis of various porous materials bearing encapsulated guests has become a popular research topic in recent years in the areas of supramolecular and materials chemistry mainly due to a variety of unique functional properties of the obtained materials.[1-11] By exploring different intramolecular weak interactions or physical adsorption methods, it is possible to insert the up-conversion nanoparticles,[12-16] metal nanoparticles,[17-20] and diverse molecular guests into the host structure.[21-25] Such an approach may lead to the generation of novel materials that combine possible advantages of the guest and host. In fact, a variety of host-guest systems have found importance in the fields of biosensing,[26-29] selective catalysis,[2-4, 10, 19, 20] and drug delivery.[30-32]

Lanthanide based metal-organic frameworks (Ln-MOFs) and coordination polymers (Ln-CPs) are ideal candidates for guest loading due to their special luminescent properties (namely, luminescent lifetimes, narrow emission bands, high luminescence quantum yields and large Stokes shifts) and unique structural features owing to high coordination numbers and versatility of Ln^{3+} ions. [33, 34] The pores in MOFs or CPs can be considered as a storage space[35, 36] or recognition sites.[36-38] The molecules that well fit the pore size could be captured by various physical and chemical processes (e.g., gas adsorption, ion exchange, self-assembly). Furthermore, these ways could be very effective encapsulation methods.

The design of suitable organic building block to achieve the encapsulation of certain types of guests is also a significant aspect to consider. As mentioned in prior literature,[39,40] bent and flexible ligands are particularly suitable for the construction of porous metal-organic networks. Moreover, organic building blocks bearing an aromatic carboxylate functionality can become good candidates for the assembly of Ln^{3+} ions into MOFs or CPs. Meanwhile, the combination of π conjugate systems of aromatic and heterocyclic rings can effectively transfer energy to the rare-earth ions, which is wieldy known as the "antenna effect". [41, 42]

[a] Key Laboratory of Nonferrous Metals Chemistry and Resources Utilization of Gansu Province and State Key Laboratory of Applied Organic Chemistry, College of Chemistry and Chemical Engineering, Lanzhou University, Lanzhou 730000, P. R. China
[b] Centro de Química Estrutural, Complexo I, Instituto Superior Técnico, Universidade de Lisboa, Av. Rovisco Pais, 1049-001, Lisbon, Portugal.

†Electronic Supplementary Information (ESI) available: anion exchange experimental details and results, additional emission spectra and structural representations, thermogravimetric analysis plots, UV-vis and IR spectra, PXRD patterns, and selected bonding parameters for **1–10**; Tables SI1–SI5 and Figures SI1–SI9. See DOI: 10.1039/b000000x/

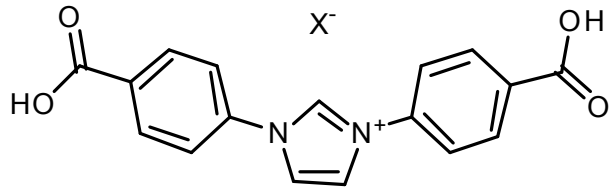

Figure 1. Structural Formula of Main Building Block $H_2Bcpi^+X^-$; X = Cl, Br. In all compounds **1**–**10**, the derived ligand Bpci is fully deprotonated and has an overall charge (1–).

Combine these two aspects, we use an imidazole ring modified by two aromatic carboxylates to build V typed ligand, on one hand, both the bent property and good antenna effect could be satisfied on the design. On the other hand, the positive charge of imidazole could attract negative charge particles such as halide anion, which could be used in the extraction of halogen anions and preparation flame retardant material. In the present study, we focused on the 1,3-bis(4-carboxyphenyl) imidazolium(1+) ligand used in a form of chloride ($H_2Bcpi^+Cl^-$) or bromide ($H_2Bcpi^+Br^-$) precursor. This building block was applied for the assembly of Ln-CPs with Eu(III) and Tb(III) ions under hydro(solvo)thermal conditions, resulting in the generation of nine new lanthanide coordination polymers with a general formula of $\{[Ln(Bcpi)_2(H_2O)]Br_xCl_{1-x}\cdot(H_2O)\}_n$ {Ln = Eu (**1**–**3**), Tb (**4**–**6**) and Gd (**7**–**9**); x = 0, 0.5, 1}. Besides, a series of heterobimetallic Tb/Eu coordination polymers $\{[Tb_{1-x}Eu_x(Bcpi)_2(H_2O)]Cl\cdot(H_2O)\}_n$ (**10**) was synthesized in a similar way by varying the content of different lanthanide ions. Thus, we describe herein the synthesis, characterization, structural features, and notable luminescent properties of these Ln-CPs materials.

Experimental Section

Materials and Physical Measurements

All the materials were purchased from commercial sources and used without further purification. The single-crystal X-ray diffraction data were collected on a Bruker SMART 1000 CCD diffractometer operating at 48 kV and 30 mA by using a graphite-monochromated Mo-Kα radiation source (λ = 0.71073 Å). An empirical absorption correction based on a comparison of redundant and equivalent reflections was applied by using SADABS. All of the structures were solved by direct methods using SHELXTL-97[43] and refined by full-matrix least-squares cycles on F2. All the non-hydrogen atoms were refined anisotropically. X-ray powder diffraction data were collected on PANalytical X'Pert Pro Diffractometer operated at 40 kV and 40 mA with Cu Kα radiation (λ = 1.5406Å).

The steady-state luminescence spectra and lifetime measurements were measured on an Edinburgh Instruments FSL920 fluorescence spectrometer, with a 450 W Xe arc lamp as the steady-state excitation source or Nd-pumped OPOlette laser as the excitation source for lifetime measurements. The quantum yields of the compounds in the solid state were determined according to an absolute method of Wrighton using an integrating sphere (150 mm diameters, $BaSO_4$ coating) from Edinburgh Instruments FLS920. The UV-Vis spectra were measured on an Agilent Technologies Cary 5000 Series UV-Vis-

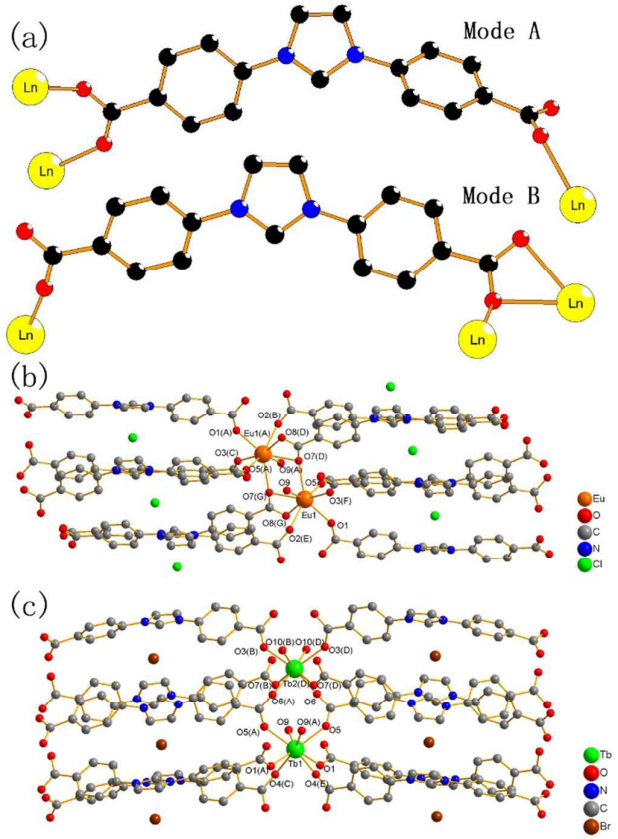

Figure 2. **(a)** Two typical coordination modes of Bcpi ligands observed in compounds 1–9. **(b)** Coordination environment in 1. The relevant equivalent-position: (A)-x,-1-y,-1-z. (B)1+x,y,z. (C)2+x,y,1+z. (D)-1-x,-1-y,-2-z. (E)-1-x,-1-y,-1-z. (F)-2-x,-1-y,-2-z. (G)1+x,y,1+z. **(c)** Coordination environment in 6. The relevant equivalent-position: (A) –x,y,0.5-z. (B)-0.5+x,0.5-y,-0.5+z. (C)-0.5+x,1.5-y,-0.5+z. (D)0.5-x,0.5-y,1-z. (E)0.5-x,1.5-y,1-z.

NIR spectrophotometer. The infrared spectra were recorded on a Burker VERTEX 70 FTIR spectrometer using KBr pellets in the 400–4000cm^{-1} region. The phosphorescence spectra were measured on a Hitachi F-4500 spectrophotometer at 77 K by distributing the solid powder in a mixed solution of methanol–ethanol (1:1, v/v).

Synthesis of $H_2Bcpi^+Cl^-$ and $H_2Bcpi^+Br^-$.

1,3-Bis(4-carboxyphenyl)imidazolium chloride ($H_2Bcpi^+Cl^-$) and bromide ($H_2Bcpi^+Br^-$) were obtained by following the reported literature procedures.[44, 45]

Synthesis of $\{[Eu(Bcpi)_2(H_2O)]Cl\cdot(H_2O)\}_n$ (1).

A 20 mL glass vial was charged with $EuCl_3\cdot6H_2O$ (0.0218 g, 0.06 mmol), $H_2Bcpi^+Cl^-$ (0.0136g, 0.04 mmol), DMF (2 mL), isopropyl alcohol (1 mL) and distilled water (1 mL). The obtained mixture was heated at 85 °C for 24 h. After cooling to room temperature, the resulting light yellow plate-like crystals were filtered off,

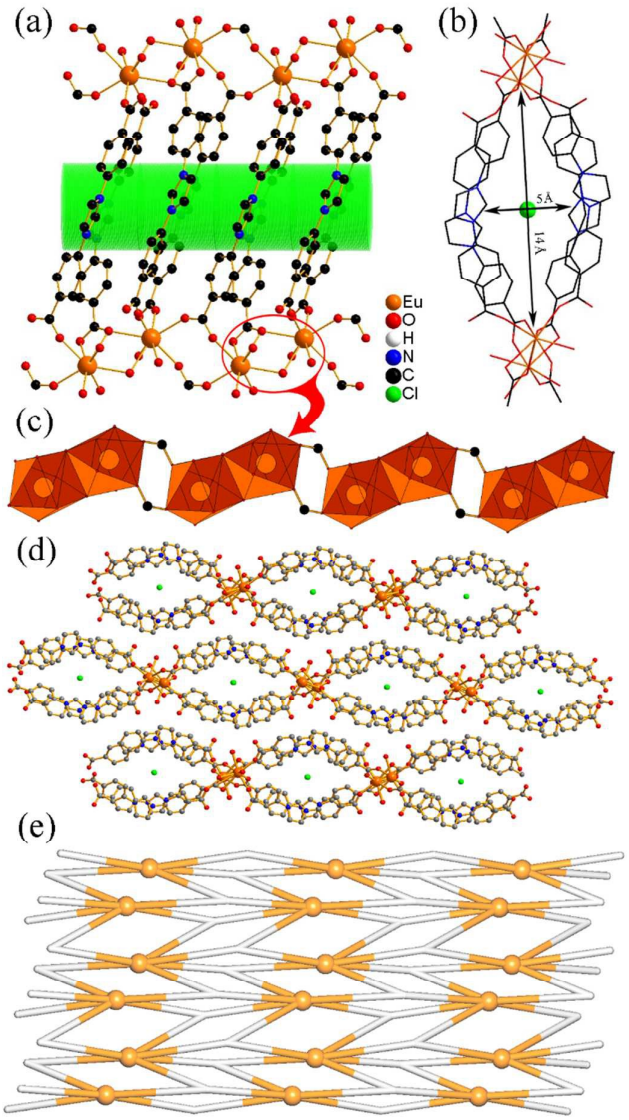

Figure 3. Structural fragments of **1**. (a) View of the 2D metal-organic layer along the *b* axis direction. (b) 1D channel shown along the *a* direction. (c) 1D Eu_2 chain motif showing coordination polyhedra of Eu atoms (view paralleled to 1D channel). (d) Packing diagram along the *a* axis showing three adjacent 2D layers. (e) Topological representation (made by topos 4.0 software) of the underlying 2D layer displaying a binodal 3,6-connected network with the **kgd** topology; rotated view along the *b* axis; colour codes: 6-connected Eu nodes (orange) and centroids of 3-connected Bcpi nodes (grey).

washed with ethanol and dried in vacuum to give **1** in 60% yield based on Eu^{3+}. IR (KBr pellet, cm^{-1}): 504 (m), 553(w), 615 (m),
692 (m), 782 (s), 860 (w), 1016 (w), 1067 (m), 1404 (vs), 1549 (vs), 1609 (vs), 2362 (vw), 2924 (w), 3101 (w), 3481 (m). Elemental analysis (%): Found: N 6.40, C 47.92, H 2.93; calculated for $C_{34}H_{26}N_4O_{10}EuCl$: N 6.68, C 48.73, H 2.89.

Synthesis of $\{[Eu(Bcpi)_2(H_2O)]Br_{0.5}Cl_{0.5}\cdot(H_2O)\}_n$ (2).

The procedure was the same as that for **1** except that $H_2Bcpi^+Cl^-$ was replaced by $H_2Bcpi^+Br^-$ (0.0156g, 0.04 mmol). Yield: 56% based on Eu^{3+}. IR (KBr pellet, cm^{-1}): 520 (m), 553 (w), 620 (m), 692 (m), 782 (s), 854 (w), 1022 (w), 1066 (m), 1253 (m), 1404 (vs), 1544 (vs), 1608 (vs), 2924 (vw), 3145 (w), 3440 (m).

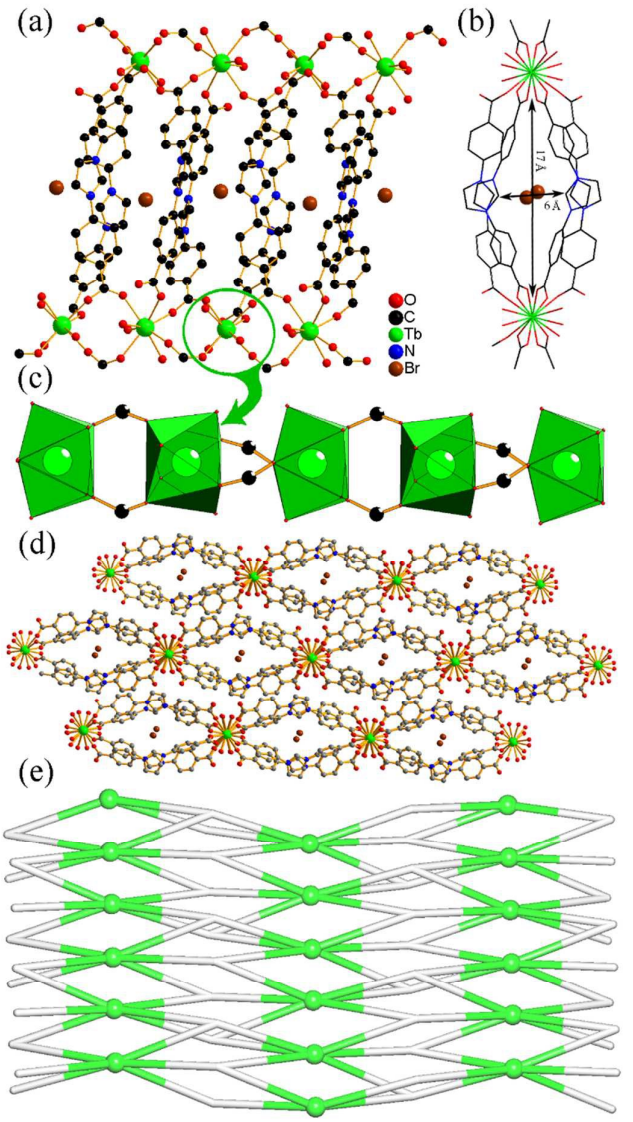

Figure 4. Structural fragments of **6.** (a) View of the 2D metal-organic layer along the *a* axis direction. (b) 1D channel of **1** along the *b* axis direction. (c) 1D Tb chain motif showing coordination polyhedra of Tb atoms (view paralleled to the 1D channel. (d) Packing diagram along the *b* axis showing three adjacent 2D layers. (e) Topological representation (made by topos 4.0 software) of the underlying 2D layer displaying a binodal 3,6-connected network with the **kgd** topology; rotated view along the *b* axis; colour codes: 6-connected Tb nodes (green) and centroids of 3-connected Bcpi nodes (grey).

Elemental analysis (%): Found: N 6.34, C 47.32, H 2.89; calculated for $C_{68}H_{52}N_8O_{20}Eu_2BrCl$: N 6.51, C 47.47, H 2.81.

Synthesis of $\{[Eu(Bcpi)_2(H_2O)]Br\cdot(H_2O)\}_n$ (3).

The procedure was the same as that for **1** except that $EuCl_3\cdot 6H_2O$ and $H_2Bcpi^+Cl^-$ were replaced by $EuBr_3\cdot 6H_2O$ (0.0300g, 0.1 mmol) and $H_2Bcpi^+Br^-$ (0.0156g, 0.04 mmol), respectively. Yield: 65% based on Eu^{3+}. IR (KBr pellet, cm^{-1}): 511 (m), 550 (w), 617 (m), 694 (m), 781 (s), 858 (w), 1020 (w), 1063 (m), 1252 (m), 1404 (vs), 1547 (vs), 1608 (vs), 1944 (vw), 2931 (w), 3086 (w), 3153 (w), 3446 (m). Elemental analysis (%):

Found: N 6.11, C 45.82, H 2.84; calculated for $C_{34}H_{26}N_4O_{10}EuBr$: N 6.35, C 46.27, H 2.72.

Table 1. Crystal Data for Compounds **1–9**

Compound	**1**	**2**	**3**	**4**	**5**	**6**	**7**	**8**	**9**
Formula	$C_{34}H_{24}EuN_4O_9{\cdot}Cl{\cdot}H_2O$	$C_{34}H_{24}EuN_4O_9{\cdot}(Br)_{0.5}{\cdot}(Cl)_{0.5}{\cdot}H_2O$	$C_{34}H_{24}EuN_4O_9{\cdot}Br{\cdot}H_2O$	$C_{34}H_{24}TbN_4O_9{\cdot}Cl{\cdot}H_2O$	$C_{34}H_{24}TbN_4O_9{\cdot}(Br)_{0.5}{\cdot}(Cl)_{0.5}{\cdot}H_2O$	$C_{34}H_{26}TbN_4O_{10}{\cdot}Br$	$C_{34}H_{24}GdN_4O_9{\cdot}Cl{\cdot}H_2O$	$C_{34}H_{24}GdN_4O_9{\cdot}(Br)_{0.5}{\cdot}(Cl)_{0.5}{\cdot}H_2O$	$C_{34}H_{24}GdN_4O_9{\cdot}Br{\cdot}H_2O$
Formula mass	838.00	860.23	882.46	844.96	867.19	889.42	843.29	865.52	887.75
Crystal system	Monoclinic	Monoclinic	Monoclinic	Monoclinic	Monoclinic	Monoclinic	Monoclinic	Monoclinic	Monoclinic
Space group	$P2_1/c$	$P2_1/c$	$P2_1/c$	$P2_1/c$	$P2_1/c$	$C2/c$	$P2_1/c$	$P2_1/c$	$P2_1/c$
a/Å	8.8828(8)	8.8847(13)	8.8422(14)	8.860(5)	8.8440(12)	23.6157(17)	8.8072 (6)	8.7794 (4)	8.865(13)
b/Å	20.4075(16)	20.515(3)	20.710(4)	20.463(11)	20.509(3)	9.9206(7)	20.3895 (18)	20.4692 (8)	20.83(3)
c/Å	18.1897(15)	18.2437(18)	18.256(3)	18.141(8)	18.1951(18)	27.2126(17)	18.0976 (18)	18.1663 (7)	18.31(3)
β/(°)	111.389(5)	111.624(5)	111.944(10)	111.41(2)	111.645(5)	96.510(4)	110.985 (7)	111.260 (4)	111.81(6)
V/Å^3	3070.2(5)	3091.2(7)	3100.9(9)	3062.0(3)	3067.5(7)	6334.3(8)	3034.3 (5)	3042.4 (2)	3139 (8)
Z	4	4	4	4	4	8	4	4	4
μ/mm^{-1}	2.20	2.79	3.38	2.47	3.07	3.56	2.35	2.95	3.46
D_{calcd}/g cm^{-3}	1.813	1.848	1.89	1.833	1.878	1.865	1.846	1.890	1.878
F(000)	1672	1708	1744	1680	1716	3504	1676	1712	1748
Reflections measured	15180	21582	13622	22038	21624	16164	13131	11299	19657
Independent reflections	5268	5597	4799	5618	5613	5739	5924	5970	4622
R_1 a [I > 2σ(I)]	0.076	0.056	0.049	0.040	0.046	0.035	0.065	0.059	0.048
wR_2 b [I > 2σ(I)]	0.178	0.156	0.092	0.095	0.132	0.073	0.169	0.153	0.118
GOF on F^2	1.01	1.07	0.96	1.03	1.06	1.00	1.09	1.05	1.01
CCDC Number	1036935	1036934	1036933	1036938	1036939	1036940	1036941	1036942	1441603

Synthesis of {[Tb(Bcpi)$_2$(H$_2$O)]Cl·(H$_2$O)}$_n$ (4). The procedure was the same as that for 1 except that $EuCl_3{\cdot}6H_2O$ was replaced by $TbCl_3{\cdot}6H_2O$ (0.0224 g, 0.06 mmol) and the reaction temperature was increased to 90 °C. Yield: 58% based on Tb^{3+}. IR (KBr pellet, cm^{-1}): 501 (m), 553 (w), 615 (m), 694 (m), 781 (s), 856 (w), 1018 (w), 1066 (m), 1252 (m), 1404 (vs), 1545 (vs), 1608 (vs), 1954 (vw), 2922 (w), 3103 (w), 3487 (m). Elemental analysis (%):

Found: N 6.36, C 48.06, H 2.98; calculated for $C_{34}H_{26}N_4O_{10}TbCl$: N 6.63, C 48.33, H 2.86.

Synthesis of {[Tb(Bcpi)$_2$(H$_2$O)]Br$_{0.5}$Cl$_{0.5}$·(H$_2$O)}$_n$ (5).

The procedure was the same as that for **1** except that $EuCl_3·6H_2O$ and $H_2Bcpi^+Cl^-$ were replaced by $TbCl_3·6H_2O$ (0.0224 g, 0.06 mmol) and $H_2Bcpi^+Br^-$(0.0156g, 0.04 mmol), respectively; and the temperature was increased up to 90 °C. Yield: 51% based on Tb^{3+}. IR (KBr pellet, cm^{-1}): 503 (m), 551 (m), 617 (m), 692 (m), 783 (s), 858 (m), 1020 (w), 1065 (m), 1254 (m), 1404 (vs), 1549 (vs), 1608 (vs), 1950 (vw), 2798 (vw), 2920 (w), 3093 (w), 3483 (w). 3577 (vw). Elemental analysis (%): Found: N 6.31, C 48.04, H 2.83; calculated for $C_{68}H_{52}N_8O_{20}Tb_2BrCl$: N 6.50, C 47.71, H 2.86.

Synthesis of {[Tb(Bcpi)$_2$(H$_2$O)$_2$]Br}$_n$ (6).

The procedure was the same as that for **1** except that $EuCl_3·6H_2O$ and $H_2Bcpi^+Cl^-$ were replaced by $TbBr_3·6H_2O$ (0.0304g, 0.06 mmol) and $H_2Bcpi^+Br^-$ (0.0156g, 0.04 mmol), respectively; and the temperature was increased to 90 °C. Yield: 58% based on Tb^{3+}. IR (KBr pellet, cm^{-1}): 519 (m), 621 (m), 692 (m), 783 (s), 872 (w), 1020 (w), 1061 (m), 1252 (m), 1383 (vs), 1406 (vs), 1545 (vs), 1603 (s), 1944 (vw), 2931 (w), 3142 (m), 3450 (m). Elemental analysis (%): Found: N 6.08, C 46.13, H 2.74; calculated for $C_{34}H_{26}N_4O_{10}TbBr$: N 6.32, C 46.12, H2.73.

Synthesis of {[Gd(Bcpi)$_2$(H$_2$O)]Cl·(H$_2$O)}$_n$ (7).

The procedure was the same as that for **1** except that $EuCl_3·6H_2O$ was replaced by $GdCl_3·6H_2O$ (0.0223g, 0.06 mmol). Yield: 50% based on Gd^{3+}. IR (KBr pellet, cm^{-1}): 501 (m), 552 (w), 617 (m), 694 (m), 783 (s), 852 (w), 949 (vw), 1020 (w), 1066 (m), 1146 (w), 1255 (m), 1335 (m), 1402 (vs), 1552 (vs), 1610 (vs), 1950 (vw), 2914 (w), 2789 (w), 3091 (w), 3481 (w). Elemental analysis (%): Found: N 6.32, C 48.10, H 2.97; calculated for $C_{34}H_{26}N_4O_{10}GdCl$: N 6.64, C 48.42, H 2.87.

Synthesis of {[Gd(Bcpi)$_2$(H$_2$O)]Br$_{0.5}$Cl$_{0.5}$·(H$_2$O)}$_n$ (8).

The procedure was the same as that for **1** except that $EuCl_3·6H_2O$ and $H_2Bcpi^+Cl^-$ were replaced by $GdCl_3·6H_2O$ (0.0223g, 0.06 mmol) and $H_2Bcpi^+Br^-$ (0.0156g, 0.04 mmol), respectively. Yield: 47% based on Gd^{3+}. IR (KBr pellet, cm^{-1}): 501 (w), 550 (w), 617 (w), 694 (w), 781 (s), 850 (w), 1016 (w), 1066 (m), 1250 (m), 1398 (vs), 1552 (vs), 1608 (vs), 1952 (vw), 2922 (w), 3485 (m). Elemental analysis (%): Found: N 6.27, C 47.90, H 2.94; calculated for $C_{68}H_{52}N_8O_{20}Gd_2BrCl$: N 6.47, C 47.18, H 2.81.

Synthesis of {[Gd(Bcpi)$_2$(H$_2$O)]Br·(H$_2$O)}$_n$ (9).

The procedure was the same as that for **1** except that $EuCl_3·6H_2O$ and $H_2Bcpi^+Cl^-$ were replaced by $GdBr_3·6H_2O$ (0.0303g, 0.06 mmol) and $H_2Bcpi^+Br^-$ (0.0156g, 0.04 mmol), respectively. Yield: 51% based on Gd^{3+}. IR (KBr pellet, cm^{-1}): 515 (w), 550 (w), 619 (w), 692 (w), 783 (s), 856 (w), 1020 (w), 1065 (w), 1250 (m), 1406 (vs), 1551 (vs), 1608 (vs), 2933 (vw), 3458 (m). Elemental analysis (%): Found: N 6.04, C 45.36, H 2.81; calculated for $C_{34}H_{26}N_4O_{10}GdBr$: N 6.31, C 46.00, H 2.72.

Synthesis of {[Tb$_{1-x}$Eu$_x$(Bcpi)$_2$(H$_2$O)]Cl·(H$_2$O)}$_n$ (10).

The heterometallic Tb/Eu CPs with varying content of metals, i.e. $Tb_{1-x}Eu_x$ (x=0.001, 0.002, 0.005, 0.01, 0.02, 0.03, 0.04, 0.05, 0.1, 0.2) were synthesized similarly to compounds **1** and **4**, except for the use of a mixture of $TbCl_3·6H_2O$ and $EuCl_3·6H_2O$. The content of $TbCl_3·6H_2O$ was initially fixed to 100% and then doping with different percentage of $EuCl_3·6H_2O$ was performed. The yields were 40% based on used lanthanide salts. The compounds were isolated as pale yellow crystals. Their IR spectra are given in Figure SI8, Supporting Information.

Results and Discussion

Description of the structures

The compounds **1–9** are isostructural and feature 2D metal-organic networks driven by μ_3-Bcpi spacers. The single crystal X-ray diffraction analyses (Table 1) reveal that **1–5** and **7–9** crystallize in the monoclinic system and space group P21/c, whereas **6** belongs to C2/c space group. Herein, only the structures of **1** (Figure 3) and **6** (Figure 4) are discussed in detail as representative examples.

Hence, the asymmetric unit of **1** contains one Eu^{3+} ion, two μ_3-Bcpi ligands, one chloride anion, one coordinated water ligand and one crystallization water molecule. As shown in Figure 2b, the eight-coordinate Eu^{3+} centres adopt a distorted $\{EuO_8\}$ dodecahedral coordination environment, filled by seven Bcpi oxygen atoms (O1, O2, O3, O5, O7, O7' and O8) and one water oxygen atom (O9). Two symmetry non-equivalent Bcpi(1–) ligands are doubly deprotonated and act as μ_3-spacers between adjacent europium centres. In Bcpi moieties, the carboxyl groups adopt either the μ_1-η^1:η^1 and η^1:η^0 coordination modes (Mode A, Figure 2a) or the μ_2-η^2:η^1 and η^1:η^0 modes (Mode B). The Eu–O distances are in the 2.324(1)–2.573 (1) Å range and are close to those found in other eight-coordinate Eu^{3+} derivatives.[46, 47] Every Bcpi ligand binds to three Eu^{3+} ions with the shortest Eu…Eu separation of 4.0431(9) Å (Table SI1). If a dot D_1 is located at the center of mass of the imidazole ring, the angle of 146.84° can be observed between the imidazole and two phenyl carboxylate functionalities in coordination Mode A. The same angle is 145.09° in the second Bcpi moiety corresponding to the coordination Mode B. The adjacent europium atoms are assembled into the Eu_2 units that are further extended into 1D chain motifs (Figure 3c). The two kinds of Bcpi ligands along with the Eu_2 units form 1D channels with the 14 × 5 $Å^2$, which was approximately measured by Mercury 3.0 program. The porosity of 7.8% was estimated by using the PLATON program (without taking into consideration the Cl^- anions and solvent molecules). The adjacent 1D chain motifs are extended into the 2D metal-organic layers by the second coordination site of each Bcpi spacer (Figure 3d). It should be mentioned that compound **2** is essentially similar to **1,** except that the guest chloride and bromide anions are alternately arranged in the channel.

To get additional insight into the structure of **1**, we carried out its topological analysis following the concept of the simplified underlying net.[48, 49] Such a net (Figure 3e) was generated after omitting terminal H_2O ligands and reducing the μ_3-Bcpi moieties to their centroids, thus resulting in a binodal 3,6-connected layer. This layer features the **kgd** [Shubnikov plane net (3.6.3.6)/dual] topology with the point symbol of $(4^3)_2(4^6.6^6.8^3)$, wherein the (4^3) and $(4^6.6^6.8^3)$ indices correspond to the 3-connected μ_3-Bcpi and 6-connected Eu nodes, respectively.

Although the structure of a 2D coordination polymer **6** resembles that of **1**, there are some differences. The asymmetric unit of **6** bears two distinct Tb1 and Tb2 atoms (half of each), two Bcpi ligands, two coordination water molecules (vs. one coordinated and one crystallization H_2O in **1**) and one bromide anion. Both eight-coordinate Tb1 and Tb2 centres are surrounded by six oxygen atoms from Bcpi moieties and two coordination water molecules, also forming a dodecahedral geometry. Both Bcpi ligands link terbium atoms only in mode A (Figure 2a) and the Tb–O bond lengths are in the 2.281(1)–2.467(1) Å range. Similarly to compound **1**, the neighboring Tb^{3+} ions are linked by the Bcpi resulting in 1D chain motifs. The angles observed between imidazole and two phenyl carboxylate functionalities of Bcpi in **6** are 143.03 and 143.68°. After omitting the bromide and hydrogen atoms, the channel was formed by two Tb-Bcpi 1D chain motifs with the size of 17 × 6 $Å^2$ and the porosity of 6.6% by utilizing Mercury 3.0 and PLATON software, respectively. Unlike compound **1**, the guest bromide anions in **6** were arranged in a terraced chain of the channel and the bromide atom is linked by weak C–H…Br hydrogen bonds with the Bcpi moieties. The 1D Tb^{3+} chain motifs and tunnels connected by Bcpi are arranged alternately, constructing a new 2D metal-organic layer. From the topological viewpoint, the underlying 2D network of **6** can also be classified as a binodal 3,6-connected layer with the **kgd** topology (Figure 4e). However, a minor difference with the topological network of **1** concerns the presence of all Tb nodes of **6** in one plane, whereas the Eu nodes of **1** are alternately positioned within two planes.

Thermogravimetric analysis

The stabilities of compounds **1–9** were examined by thermogravimetric analyses (TGA) in air atmosphere in the temperature range of 20–800 °C. The results indicate that all the compounds show a similar thermal behavior owing to their isomorphous structures. Thus, only the thermal stability of **1** is discussed in detail. The TG curve of **1** displays the loss of one coordination and one crystallization water molecules on heating up to 140 °C with the observed weight loss of 4.1% (calculated weight loss is 4.4%). After removal of water, the compound apparently remains stable up to 440 °C. Above this temperature, the decomposition of metal-organic network occurs. These data indicate that the imidazolium-based compounds have a good thermal stability (see also Supporting Information, Figure SI5).

Photoluminescent Properties

The transient and steady-state photoluminescence spectra of **1–6** were collected on the crystalline samples at room temperature. The emission spectra of Eu coordination polymers **1–3** (Eu-CPs) and Tb coordination polymers **4–6** (Tb-CPs) were measured at the excitation wavelength of 310 and 312 nm, respectively. As shown in Figure 5, the emission spectra of **1–3** reveal five characteristic emission lines, namely at 579, 591, 617, 652 and 701 nm owing to the $^5D_0 \rightarrow {}^7F_J$ (J=0-4) transitions, respectively. The emission spectra of **4–6** exhibit four sharp peaks with the maxima at 487, 544, 582 and 619 nm, resulting from the $^5D_4 \rightarrow {}^7F_J$ (J=6-3) transitions, respectively. It is worthwhile to note that the increasing content of bromide in the crystalline solids of **1–6** could enhance the photoluminescence intensity of both Eu-CPs and Tb-CPs. As shown in Figure 5a**,** compound **1** exhibits a low luminescent emission intensity. The photoluminescence quantum yield (Φ) of **2** is significantly enhanced to 15.80% (4.5-fold increase) if compared to that (3.50%) of compound **1**, while the bromide content increases from 0 in **1** to 4.64% in **2**. When $EuBr_3$ and $H_2Bcpi^+Br^-$ are used to obtain compound **3**, Φ enhances from 15.80 to 23.46% (1.5-fold increase) in comparison with compound **2** (with the bromine content raising from 4.64 to 9.05%). Compounds **4–6** show essentially similar features. The enhancement of Φ increases from 3.08% (for **4**) to 13.83% (for **5**) and then to 19.63% (for **6**). It is also increased by 4.5-fold and 1.4-fold, respectively, by using compound **4** as datum. The above results should be attributed to the intra-heavy-atom effect.[50-54] The observed life time in case of Eu^{3+} compounds **1–3** is about 501 (**1**), 572 (**2**) and 583 (**3**) μs, whereas that of Tb compounds **4–6** is 716 (**4**), 825 (**5**) and 894 (**6**) μs. These lifetime data were determined by monitoring the $^5D_0 \rightarrow {}^7F_2$ and $^5D_4 \rightarrow {}^7F_5$ lines, respectively. In isostructural compounds **1–3**, all the crystal structure parameters are analogous (Table 1) and the only difference concerns the type of the halogen guest in the cationic host channels. This phenomenon indicates that the bromide guests could well induce photoluminescent enhancement and its efficiency can be better than that of the chloride anion. In Tb-CPs, the structure of **6** was slightly different from compounds **4** and **5,** and the photoluminescent properties were consistent with the Eu-CPs. The angle of $\angle C_8Eu_1C_{25}$ in Eu-Cps (Figure SI12) shows that with the increasing of the volume of halogen (from Cl to Br) the rigidity of structure is also increasing. The presence of a halogen atom could affect the rate of population from singlet to triplet state via increasing volume of halogen anions.[29, 55-57]

To demonstrate the ligand sensitization of lanthanide ions, the phosphorescence spectrum of **7-9** (see Figure SI2) and absorption spectrum of **7-9** (see Figure SI3) were collected. The Uv-vis spectrum shows that the absorbance edge of compound **7-9** are 31949cm^{-1} (313nm), 31746cm^{-1} (315m) and 31746cm^{-1} (315nm) respectively. The triplet energy level of ligand Bcpi-X have been declared by measuring phosphorescence spectrum of 7-9 in methanol–ethanol solution (1:1 v/v) at 77K. According to the test, the triplet

energy level of Bcpi-X in **7-9** are 20325cm^{-1} (492nm), 20450cm^{-1} (488nm), and 21739cm^{-1} (460nm) respectively. Based on the Reinhoudt's empirical rule,[58] the ligand-to-metal energy transfer becomes effective when $\Delta E_{Bcpi}(^1\pi\pi^* - ^3\pi\pi^*)$ is at least 5000 cm^{-1} and the long wavelength absorption edge of the antenna must be below 346nm for Tb^{3+} and 385nm for Eu^{3+}. Both Eu-Cps and Tb-Cps are in accordance with the conclusion which means the sensitization efficiency of Eu^{3+} and Tb^{3+} is good.

As shown in Figure 5, the sensitization pathway in **1-6** can be described as following steps: 1) the excitation of ligands into their excited singlet states; 2) ISC of ligands to their triplet states; 3) energy transfer from ligand to ^5D_j of lanthanide ions; 4) the transitions to the ground state with luminescence emission.

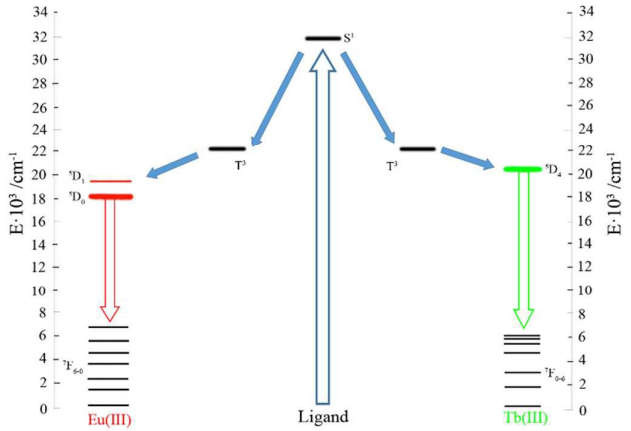

Figure 5. The schematic energy level diagram and the energy transfer process of **1-6**

According to the Judd–Ofelt Theory, [59-63] the sensitization efficiency (η_{sens}) regarding the ligand in compounds **1–3** could be calculated by the following equations:

$$\Phi_{tot} = \eta_{sens}\Phi_{Ln} \quad (1)$$

$$\Phi_{Ln} = {}^{\tau_{obs}}/_{\tau_{RAD}} \quad (2)$$

$$\frac{1}{\tau_R} = A_{MD,0} * n^3({}^{I_{tot}}/_{I_{MD}}) \quad (3)$$

In these equations, Φ_{tot} is the total quantum yield; Φ_{Ln} is the lanthanide quantum yield; *n* is the refractive index of experiment medium (in a solid coordination compound, this value is usually equal to 1.5);[64] τ_{obs} is the observed fluorescence life time; I_{tot} / I_{MD} represent the specific value regarding the integration of total area and the $^5D_0 \rightarrow {}^7F_1$ band area of compounds **1–3** (Figure 5). Among them, Φ_{tot}, τ_{obs}, I_{tot} and I_{MD} can be obtained by experiments. For compounds **1–3**, the η_{sens} is 0.076, 0.284 and 0.476, respectively. Further details can be seen in Table SI2.

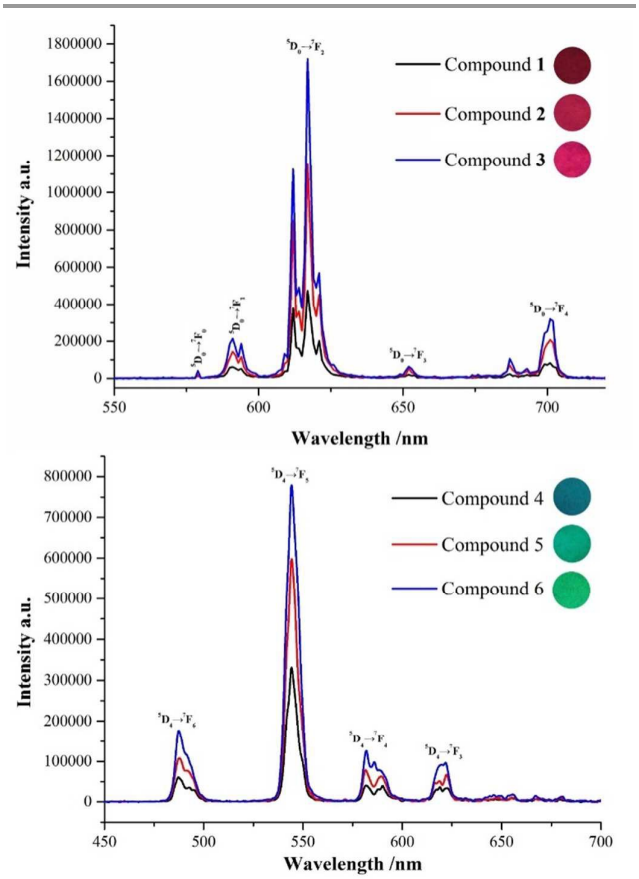

Figure 6. The emission spectra for compounds **1–3** (top) and **4–6** (bottom) recorded using the crystalline samples at room temperature. The top right corner of each picture is the material color under 365 nm ultraviolet excitation.

The heterobimetallic $Tb_{1-x}Eu_x$ {x is in the 0.001–0.2 range} coordination polymers **10** exhibit both Eu(III) and Tb(III) based emissions (Figure 6). When the doping ratios of Eu(III) and Tb(III) were adjusted, the change of emission intensities could be observed, and the emission color transformation could be realized between green and red. According to Figure 6, the CIE chromaticity diagrams of these doped materials indicate that the emission color of the doped materials could be tuned into the yellow area. According to the Inductively Coupled Plasma (known as ICP) results, the color coordinates could be described as linear; the emission of the obtained materials could be easily modified by changing the ratio of Eu(III) and Tb(III).

Anion exchange experiment

The encapsulation stability of halogen anions was tested by the anion exchange experiment. The chosen halogen and pseudohalogen anions (Br^-, I^-, CN^-, SCN^-, N_3^-) with a certain concentration gradient were introduced into a suspension of a fine powder of **1** in DMF; then the mixture was subjected to a 30 min ultrasonic oscillation and heated to 90 ℃ for 72 h. After cooling to room temperature, the light yellow suspensions were analysed by using a Hitachi F-7000 spectrophotometer for photoluminescence. The test condition

was the same as for compound **1** and is listed in the Supporting Information.

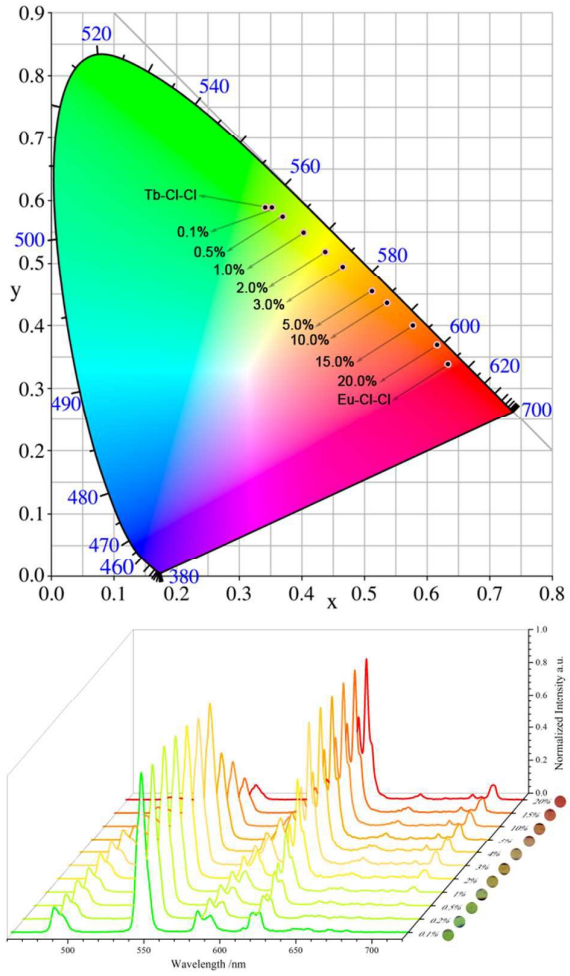

Figure 7. The CIE1931 chromaticity diagram (top) and the emission spectra (bottom) of the heterobimetallic Tb/Eu compounds with different content of metals. The right side is the real color of the material under the 365 nm ultraviolet excitation.

The obtained results indicate that the exogenous anions cannot exchange the encapsulated halogen anions. The pseudohalogen anions can hardly affect the luminescence of **1**. The SCN- , to some extent, can slightly affect the $^5D_0 \rightarrow {}^7F_2$ and $^5D_0 \rightarrow {}^7F_1$ transitions The CN^- and N_3^- have no influence on the photoluminescence in the range of 450-700 nm. The Br^- shows the same result as SCN^- due to the effect of external heavy atom. However, interestingly, I^- shows only a slight enhancement of $^5D_0 \rightarrow {}^7F_2$. The reason for that is the electric dipole transition, $^5D_0 \rightarrow {}^7F_2$ of Eu (III) which can be easily affected by the outside coordination environment but the magnetic dipole transition $^5D_0 \rightarrow {}^7F_1$ was insensitive to the coordination environment.

Conclusions

In summary, by predesign of ligand, nine new 2D lanthanide homometallic coordination polymers were successfully synthesized and fully characterized, showing an encapsulation of halide anions in the metal-organic channels constructed from lanthanide and 1,3-bis(4-carboxyphenyl)imidazolium nodes. Single-crystal X-ray data reveal that all the obtained compounds are isostructural and feature cationic 2D metal-organic layers, which can be topologically classified as the **kgd** underlying nets.

It was found that the guest halogen encapsulation could effectively improve the photoluminescent intensity, quantum yield and sensitization efficiency of the ligand in the obtained Eu(III) or Tb(III) coordination polymers. The increasing content of bromide in the crystalline solids of **1**–**6** could enhance the quantum yield 6.7-fold overall increase in Eu-CPs and 6.3-fold overall increase in Tb-CPs. Furthermore, a series heterometallic Eu/Tb color tunable luminescent materials was prepared by *in situ* doping method, allowing to continuously tune the emission color from green to red with respect to the relative content of Eu(III) ions. The observed findings can be of potential significance towards the development of novel yellow light tunable materials.

Acknowledgements

The authors acknowledge financial support from the National Natural Science Foundation of China (21431002 and 91122007) and the Specialized Research Fund for the Doctoral Program of Higher Education (20110211130002).

Notes and references

‡ *Key Laboratory of Nonferrous Metals Chemistry and Resources Utilization of Gansu Province and State Key Laboratory of Applied Organic Chemistry, College of Chemistry and Chemical Engineering, Lanzhou University, Lanzhou 730000, P. R. China*

Email:liuws@lzu.edu.cn Tel: +86 931-8915151

‡ *Centro de Química Estrutural, Complexo I, Instituto Superior Técnico, Universidade de Lisboa, Av. Rovisco Pais, 1049-001, Lisbon, Portugal.*

†Electronic Supplementary Information (ESI) available: anion exchange experimental details and results, additional emission spectra and structural representations, thermogravimetric analysis plots, UV-vis and IR spectra, PXRD patterns, and selected bonding parameters for **1**–**9**; Tables SI1–SI5 and Figures SI1–SI12. See DOI: 10.1039/b000000x/

1. H. S. El-Sheshtawy, B. S. Bassil, K. I. Assaf, U. Kortz and W. M. Nau, *J Am Chem Soc*, 2012, **134**, 19935-19941.
2. S. Zarra, D. M. Wood, D. A. Roberts and J. R. Nitschke, *Chem Soc Rev*, 2015, **44**, 419-432.
3. J. N. Rebilly, B. Colasson, O. Bistri, D. Over and O. Reinaud, *Chem Soc Rev*, 2015, **44**, 467-489.
4. S. H. Leenders, R. Gramage-Doria, B. de Bruin and J. N. Reek, *Chem Soc Rev*, 2015, **44**, 433-448.
5. K. Kobayashi and M. Yamanaka, *Chem Soc Rev*, 2015, **44**, 449-466.
6. J. H. Jordan and B. C. Gibb, *Chem Soc Rev*, 2015, **44**, 547-585.

7. G. Yu, K. Jie and F. Huang, *Chem Rev*, 2015.
8. W. L. Leong and J. J. Vittal, *Chem Rev*, 2011, **111**, 688-764.
9. C. J. Brown, F. D. Toste, R. G. Bergman and K. N. Raymond, *Chem Rev*, 2015, **115**, 3012-3035.
10. H. Amouri, C. Desmarets and J. Moussa, *Chem Rev*, 2012, **112**, 2015-2041.
11. S. R. Seidel and P. J. Stang, *Accounts of Chemical Research*, 2002, **35**, 972-983.
12. Y. I. Park, K. T. Lee, Y. D. Suh and T. Hyeon, *Chem Soc Rev*, 2015, **44**, 1302-1317.
13. D. Yang, P. Ma, Z. Hou, Z. Cheng, C. Li and J. Lin, *Chem Soc Rev*, 2015, **44**, 1416-1448.
14. X. Li, F. Zhang and D. Zhao, *Chem Soc Rev*, 2015, **44**, 1346-1378.
15. J. Zhou, Z. Liu and F. Li, *Chem Soc Rev*, 2012, **41**, 1323-1349.
16. D. L. Inglefield, T. R. Merritt, B. A. Magill, T. E. Long and G. A. Khodaparast, *J. Mater. Chem. C*, 2015, **3**, 5556-5565.
17. M. Pittelkow, T. Brock-Nannestad, K. Moth-Poulsen and J. B. Christensen, *Chem Commun (Camb)*, 2008, 2358-2360.
18. Y. Zhou, M. Zhu and S. Li, *J. Mater. Chem. A*, 2014, **2**, 6834.
19. J. Deng, P. Ren, D. Deng, L. Yu, F. Yang and X. Bao, *Energy & Environmental Science*, 2014, **7**, 1919.
20. Y. Zhang, Y. Zhou, Z. Zhang, S. Xiang, X. Sheng, S. Zhou and F. Wang, *Dalton Trans*, 2014, **43**, 1360-1367.
21. S. Tartaggia, A. Scarso, P. Padovan, O. De Lucchi and F. Fabris, *Organic letters*, 2009, **11**, 3926-3929.
22. S. Mirtschin, A. Slabon-Turski, R. Scopelliti, A. H. Velders and K. Severin, *J Am Chem Soc*, 2010, **132**, 14004-14005.
23. M. Han, D. M. Engelhard and G. H. Clever, *Chem Soc Rev*, 2014, **43**, 1848-1860.
24. R. Sarma, H. Deka, A. K. Boudalis and J. B. Baruah, *Crystal Growth & Design*, 2011, **11**, 547-554.
25. R. Sarma and J. B. Baruah, *Journal of Coordination Chemistry*, 2010, **63**, 457-463.
26. W. Liu, T. Jiao, Y. Li, Q. Liu, M. Tan, H. Wang and L. Wang, *J Am Chem Soc*, 2004, **126**, 2280-2281.
27. J. Rocha, L. D. Carlos, F. A. Paz and D. Ananias, *Chem Soc Rev*, 2011, **40**, 926-940.
28. K. Ariga, H. Ito, J. P. Hill and H. Tsukube, *Chem Soc Rev*, 2012, **41**, 5800-5835.
29. J. X. Ma, X. F. Huang, X. Q. Song and W. S. Liu, *Chemistry*, 2013, **19**, 3590-3595.
30. L. Schoonen and J. C. van Hest, *Nanoscale*, 2014, **6**, 7124-7141.
31. Y. R. Zheng, K. Suntharalingam, T. C. Johnstone and S. J. Lippard, *Chem Sci*, 2015, **6**, 1189-1193.
32. R. G. Mendes, A. Bachmatiuk, B. Büchner, G. Cuniberti and M. H. Rümmeli, *J. Mater. Chem. B*, 2013, **1**, 401-428.
33. K. Binnemans, *Chem Rev*, 2009, **109**, 4283-4374.
34. F. A. Paz, J. Klinowski, S. M. Vilela, J. P. Tome, J. A. Cavaleiro and J. Rocha, *Chem Soc Rev*, 2012, **41**, 1088-1110.
35. O. M. Yaghi, M. O'Keeffe, N. W. Ockwig, H. K. Chae, M. Eddaoudi and J. Kim, *Nature*, 2003, **423**, 705-714.
36. P. Horcajada, T. Chalati, C. Serre, B. Gillet, C. Sebrie, T. Baati, J. F. Eubank, D. Heurtaux, P. Clayette, C. Kreuz, J. S. Chang, Y. K. Hwang, V. Marsaud, P. N. Bories, L. Cynober, S. Gil, G. Ferey, P. Couvreur and R. Gref, *Nat Mater*, 2010, **9**, 172-178.
37. N. Yanai, K. Kitayama, Y. Hijikata, H. Sato, R. Matsuda, Y. Kubota, M. Takata, M. Mizuno, T. Uemura and S. Kitagawa, *Nat Mater*, 2011, **10**, 787-793.
38. H. B. Tanh Jeazet, C. Staudt and C. Janiak, *Dalton Trans*, 2012, **41**, 14003-14027.
39. B.-Q. Song, X.-L. Wang, G.-S. Yang, H.-N. Wang, J. Liang, K.-Z. Shao and Z.-M. Su, *CrystEngComm*, 2014, **16**, 6882.
40. S. Sen, T. Yamada, H. Kitagawa and P. K. Bharadwaj, *Crystal Growth & Design*, 2014, **14**, 1240-1244.
41. E. G. Moore, A. P. Samuel and K. N. Raymond, *Acc Chem Res*, 2009, **42**, 542-552.
42. J. C. Bunzli, *Chem Rev*, 2010, **110**, 2729-2755.
43. G. M. Sheldrick, *Acta Crystallogr A*, 2008, **64**, 112-122.
44. R. S. Crees, M. L. Cole, L. R. Hanton and C. J. Sumby, *Inorg Chem*, 2010, **49**, 1712-1719.
45. S. Sen, N. N. Nair, T. Yamada, H. Kitagawa and P. K. Bharadwaj, *J Am Chem Soc*, 2012, **134**, 19432-19437.
46. G. Dong, L. Yu-Ting, D. Chun-Ying, M. Hong and M. Qing-Jin, *Inorg Chem*, 2003, **42**, 2519-2530.
47. J. L. Song and J. G. Mao, *Chemistry*, 2005, **11**, 1417-1424.
48. V. A. Blatov, *IUCr CompComm Newsletter*, 2006, **7**, 4-38.
49. V. A. Blatov, A. P. Shevchenko and D. M. Proserpio, *Crystal Growth & Design*, 2014, **14**, 3576-3586.
50. J. C. Koziar and D. O. Cowan, *J Am Chem Soc*, 1976, 1001-1007.
51. A. K. Chandra, N. J. Turro, A. L. L. Jr. and P. Stone, *J Am Chem Soc*, 1978, 4964-4968.
52. G. W. Suter, A. J. Kallir, U. P. Wild and T. Vodinh, *Anal Chem*, 1987, **59**, 1644-1646.
53. V. Martinez-Martinez, R. Sola Llano, S. Furukawa, Y. Takashima, I. Lopez Arbeloa and S. Kitagawa, *Chemphyschem*, 2014, **15**, 2517-2521.
54. R. Pizzoferrato, R. Francini, S. Pietrantoni, R. Paolesse, F. Mandoj, A. Monguzzi and F. Meinardi, *J Phys Chem A*, 2010, **114**, 4163-4168.
55. R. Custelcean, *Chem Soc Rev*, 2010, **39**, 3675.
56. R. Custelcean, *Chem Soc Rev*, 2014, **43**, 1813.
57. X. F. Huang, J. X. Ma and W. S. Liu, *Inorg Chem*, 2014, **53**, 5922-5930.
58. F. J. Steemers, W. Verboom, D. N. Reinhoudt, E. B. van der Tol and J. W. Verhoeven, *J Am Chem Soc*, 1995, **117**, 9408-9414.
59. M. H. V. Werts, R. T. F. Jukes and J. W. Verhoeven, *Physical Chemistry Chemical Physics*, 2002, **4**, 1542-1548.
60. N. Arnaud and J. Georges, *Spectrochimica Acta Part A: Molecular and Biomolecular Spectroscopy*, 2003, **59**, 1829-1840.
61. S. V. Eliseeva and J. C. Bunzli, *Chem Soc Rev*, 2010, **39**, 189-227.
62. J. Xu, L. Jia, Y. Ma, X. Liu, H. Tian, W. Liu and Y. Tang, *Materials Chemistry and Physics*, 2012, **136**, 112-119.
63. C. Gao, A. M. Kirillov, W. Dou, X. Tang, L. Liu, X. Yan, Y. Xie, P. Zang, W. Liu and Y. Tang, *Inorg Chem*, 2014, **53**, 935-942.
64. R. Pavithran, N. S. Saleesh Kumar, S. Biju, M. L. Reddy, S. A. Junior and R. O. Freire, *Inorg Chem*, 2006, **45**, 2184-2192.

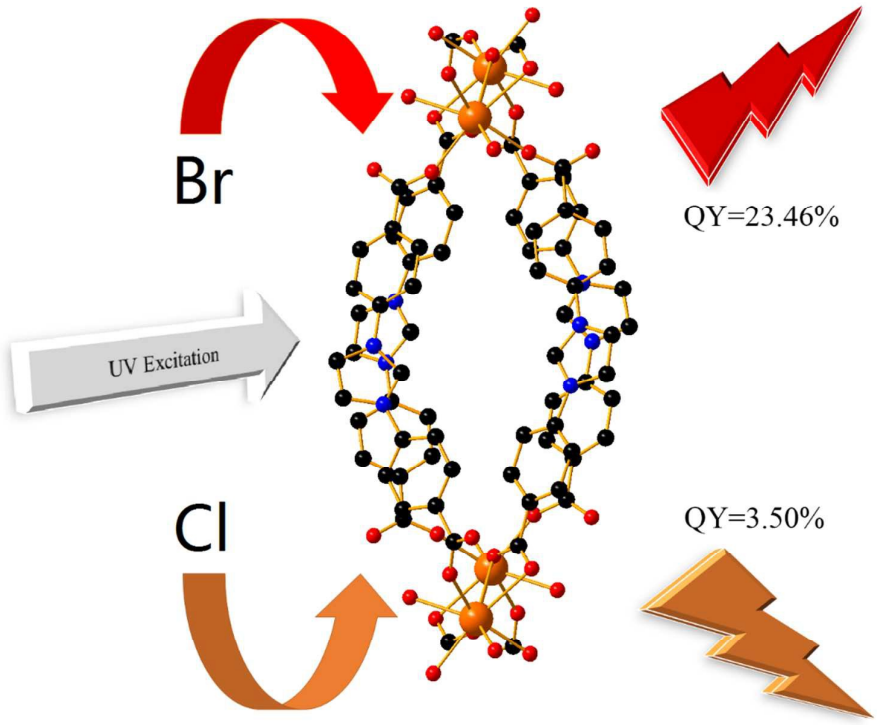

The halogen anions which encapsulated in the tunnel of the 2D lanthanide coordination polymers (Ln-CPs) could enhanced the solid-state photoluminescence.